Tensile Properties of Silicone Biocomposite Reinforced with Waste Material (*Hevea brasiliensis* Sawdust): Experimental and Numerical Approach

Noorainol Faiz Noor Haris, Mohd Azman Yahaya, and Jamaluddin Mahmud *

Hevea brasiliensis wood becomes residue at plantations in Malaysia. In this study, these residues were reinforced into silicone rubber to produce a new soft biocomposite (*Hevea brasiliensis*-silicone biocomposite). The newly introduced soft biocomposite has potential for use in cushioning and sealing applications. The specimens were prepared with five different compositions (0 wt%, 4 wt%, 8 wt%, 12 wt%, and 16 wt% fiber content). Tensile tests were conducted according to ASTM D412 (2008) to assess the mechanical properties. Morphological characteristics were analyzed from the fractured surface of specimens. Stress-stretch data was used to quantify the non-linear tensile behavior, which was based on Neo-Hookean, Mooney-Rivlin, and Ogden hyperelastic constitutive equations. An increase in fiber content improved the modulus of silicone rubber. However, it reduced the flexibility and elastic properties of the silicone rubber biocomposite. The increasing material constant values supported these findings. The hyperelastic models accurately represented the behavior of the *Hevea brasiliensis*-silicone biocomposite. This study contributes knowledge towards a better understanding of the mechanical behavior of *Hevea brasiliensis*-silicone biocomposites.

DOI: 10.15376/biores.17.3.4623-4637

Keywords: Mechanical properties; Hevea brasiliensis; Natural fiber; Biocomposite; Hyperelastic; Tensile strength

*Contact information: School of Mechanical Engineering, College of Engineering, Universiti Teknologi MARA, 40450 Shah Alam, Selangor, Malaysia; *Corresponding author: jm@uitm.edu.my*

INTRODUCTION

Hevea brasiliensis, commonly known as the rubber tree, is a hardwood from the Euphorbiaceae family. It is estimated that more than 80% of the total rubber plantation areas are in Asia; plantations in Malaysia, Thailand, and Indonesia make up 70% of the total rubber plantations (Ratnasingam *et al.* 2015). While the main product is latex, the by-product is rubber wood, which has great economic value. The wood is obtained from agricultural plantations when the rubber trees are replanted every 25 years to 30 years, due to declining latex yield (Haris *et al*. 2019). They are made into multiple products: furniture, wood panels, flooring, and indoor building components. However, 90% of the wood ends up as residues, as byproducts from furniture factories (4%), waste from sawmills (32%), and unused small branches (54%). Only 10% of the wood is fully utilized into products (Petchpradab *et al.* 2009). These wood waste products are considered as agricultural waste that need to be disposed. In Malaysia alone, about 1.2 million tons of agricultural wastes were dumped to landfills, which contribute to environmental pollution (Shaaban *et al.*

2013). Thus, incorporation of the waste into composite materials can help solve this environmental problem.

Hevea brasiliensis fiber is known to have high cellulose content of 39 wt.%. Cellulose is a linear polysaccharide with β-1,4-glycosidic linkage repeating unit. Its properties, which include high stability, tunable functionality in-build crystallinity, potential mechanical strength, and environment-friendly nature, makes them a worthy alternative material in paper, textiles, and pharmaceutical industries (Lima and Borsali 2004). Cellulose were also utilized in the making of building blocks and plastic-based composites (Moon *et al.* 2011). It is estimated that one-third of industrially produced polymers are directly or indirectly connected to cellulose (Haque *et al.* 2017). Table 1 shows the chemical composition of *Hevea brasiliensis* wood as reported in a study by (Petchpradab *et al.* 2009).

Table 1. Composition of *Hevea brasiliensis* Wood

Fiber	Cellulose (wt%)	Hemicellulose (wt%)	Lignin (wt%)	Ash (wt%)
Hevea brasiliensis	39	29	28	4

The use of plant fibers as reinforcement in composite materials has been exhaustively explored for potential applications. Besides being bio-sourced, recyclable, and biodegradable (Helaili *et al.* 2021), characteristics such as high resistance to wear and tear, high specific modulus, and light weight are the reasons they are utilized as reinforcing agents in polymers composites, including thermoplastics and thermoset (Izzah *et al.* 2022). A composite is a material that is fabricated from the combination of two or more different materials. The term biocomposite is used when the constituent is derived from a biological source, *e.g.*, plant fibers, whether it is the matrix, used as reinforcement, or both. Unique properties can be obtained as a result of the combination that cannot be obtained by the individual materials alone.

As non-renewable resources become scarcer, plant fibers are alternatives to overcome this issue. Moreover, plant fibers are preferable, as they are cheaper, biodegradable, have a low density, and are abundant in nature (Hanipah *et al.* 2020). Plant fibers can be classified as wood or non-wood. Non-wood fibers can be either fruit, bast, leaf, grass, seed, or stalk, depending on their origins. For wood fibers, they are either softwood or hardwood fibers.

Elastomers, such as silicone rubber, are one of the potential matrixes used to produce composite materials. They are known to possess excellent elasticity, low toxicity, good biocompatibility, as well as being very stable at low and high temperature (Xu *et al.* 2016). Generally, silicone rubber possesses low modulus, where a small stress applied to the silicone rubber will cause a large deformation. This limits its application to a certain extent, especially in dynamic circumstance (Feng *et al.* 2017). By adding reinforcement to the rubber, the modulus can be improved. However, other mechanical properties of silicone rubber are reduced, particularly the flexibility and elastic properties (Xu *et al.* 2010). Previous studies showed that when certain materials, such as carbon nanotubes (Wang and Cheng 2014) and graphite nanoplatelets (Raza *et al.* 2011), were reinforced into silicone rubber, its properties were improved. But there has been a lack of such studies involving plant fibers.

To date, no study has reported about the reinforcement of *Hevea brasiliensis* into silicone rubber. Therefore, this study is novel, as it introduces a newly developed silicone biocomposite material, namely *Hevea brasiliensis* – silicone biocomposite (copyrighted as HeBraC; MyIPO IP no. CRLY00026192). The current work attempts to establish the tensile properties of *Hevea brasiliensis* – silicone biocomposite through experimental and numerical approach. The numerical analysis focused on quantifying the elastic behavior by obtaining the material constant values based on three most common hyperelastic models, Neo – Hookean, Mooney – Rivlin and Ogden models.

EXPERIMENTAL

Materials and Composite Preparation

The *Hevea brasiliensis* fibers used in this research were obtained from a furniture industry located in Setia Alam, Selangor, Malaysia. The fibers were in the form of sawdust, which resulted from the trimming and planing of wood. The sawdust was crushed into a powder using a planetary mono mill and later sieved to get a uniform size (0.16 µm). After sieving, the powders were dried for 24 h at 110 °C to remove the moisture content. The temperature and time of drying process was set based on past studies in which *Hevea brasiliensis* sawdust was used in the making composites (Shaaban *et al.* 2015; Khan *et al.* 2016). A study by (Sulaiman *et al.* 2015) stated that *Hevea brasiliensis* fiber is expected to have zero moisture content after 24 h of drying process. For the matrix material, Silicone Ecoflex 00-30 (Platinum cure Silicone Rubber Compound) was selected and supplied by Castmech Sdn. Bhd. (Ipoh, Perak, Malaysia).

The specimens were prepared with five different compositions in terms of fiber content (0 wt%, 4 wt%, 8 wt%, 12 wt%, and 16 wt%). They were limited to 16 wt%, as beyond it will exceed the saturation point. Similar compositions were used by (Radzi and Mahmud 2017) and (Wu and Yu 2015) in the study of composites. The appropriate fiber content was added into the silicone solution during the stirring process. This mixture was poured into a mold and left to cure for 4 h at room temperature. Figure 1 shows the dimensions of specimens according to ASTM D412.

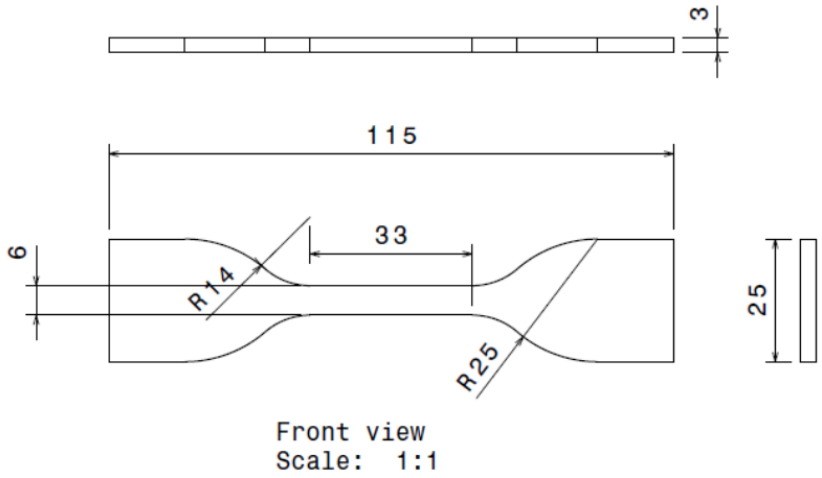

Fig. 1. Size of specimen according to ASTM D412

Tensile Testing

The tensile tests were carried out according to ASTM D412 (2008) using a 3382 universal testing machine (Instron, Norwood, MA, USA) at 100 kN. Five specimens were prepared for each of the weight compositions, and the tests were performed with a crosshead speed of 500 mm/min until failure state was reached.

Scanning Electron Microscopy (SEM)

For the morphological analysis, a TM3000 scanning electron microscope (Hitachi, Tokyo, Japan) was used to produce micrographs of the fractured surface of the specimen at 15.0 kV. The fractured surfaces were first coated with platinum using a sputter coating machine to obtain clear images.

Determining Hyperelastic Constants

Because the composites prepared in this study were soft, highly elastic, and behaved like rubbery materials, they were assumed to possess hyperelastic behavior. For this, their deformation behavior could be represented using the stress - stretch relation (σ_E - λ). Three hyperelastic constitutive equations, the Neo – Hookean, Mooney – Rivlin and Ogden models, were employed to determine the materials constants for all of the fiber compositions. The models are well described in literature (Ali *et al.* 2010). Assuming that the silicone biocomposites were incompressible, isotropic, and hyperelastic, the derived equations are shown in Eq. 1, Eq. 2, and Eq. 3 respectively,

$$\sigma_E = 2C_1\left(\lambda - \frac{1}{\lambda^2}\right) \quad (1)$$

$$\sigma_E = \frac{1}{\lambda}\left[\left(2C_1 + \frac{2C_2}{\lambda}\right)\left(\lambda^2 - \frac{1}{\lambda}\right)\right] \quad (2)$$

$$\sigma_E = \frac{\mu}{\lambda}\left(\lambda^{\alpha} - \lambda^{-\frac{\alpha}{2}}\right) \quad (3)$$

where σ_E is the engineering stress (MPa), C_1, C_2, α, and μ are the material constants (MPa), and λ is the stretch value. A similar approach was used by Bahrain *et al.* (2018). In their study the Neo – Hookean and Mooney – Rivlin models were used in quantifying the hyperelastic material constant values.

Since the equations were expressed in terms of the engineering stress - stretch relation (σ_E-λ), the data collected from the previous tensile tests was first converted into the engineering stress - stretch relation ($\underline{\sigma}_E$-λ) using Eq. 4,

$$\lambda = 1 + \varepsilon \quad (4)$$

where λ is the stretch value and ε is the strain value (m/m)

A computational procedure was developed to determine the material constant values by curve fitting the experimental data using Eqs. 1, 2, and 3.

RESULTS AND DISCUSSION

Tensile Properties

The tensile test results for all specimens were acquired, and the average readings were computed for each composition, as displayed in Table 2. It is apparent that the Young's modulus value increased as more fibers were incorporated. A higher modulus indicates that the specimens were stiffer and experienced higher resistance to being

deformed elastically when stress was applied. The increasing stiffness of the specimen was due to low polymer chain mobility of silicone rubber as a result of addition of fibers which fills up the spaces between the chains, as reported by (Ismail *et al.* 2015). A similar trend was reported by Benevides and Nunes (2015), where the stiffness of nanocomposite increased with further addition of alumina-nanoparticles. With the addition of *Hevea brasiliensis* fibers, the crosslink density of silicone rubber was altered, causing more interconnected link between polymer chains, increasing its crosslink density. This causes the material to stiffen. In contrast to the Young's modulus, other mechanical properties showed an opposite pattern. The values declined with increasing fiber content, which agrees with the trend of the graph shown in Fig. 2. The pure silicone rubber possessed the highest stretch value when compared to other specimens with higher fibers content. As *Hevea brasiliensis* fibers were introduced into the composites, it reduced the highly nonlinear elastic behavior of the silicone rubber. At a fiber composition of 12 wt%, the composites started to become stiffer, as shown by the graph displaying an almost linear curve.

Table 2. Average Results of the Tensile Tests

Properties	0 wt%	4 wt%	8 wt%	12 wt%	16 wt%
Young's modulus (MPa)	0.1165	0.1222	0.1394	0.1452	0.1992
Maximum load (N)	30.32	24.81	21.92	19.77	16.85
Tensile Stress at Maximum Load (MPa)	1.68	1.38	1.22	1.10	0.94
Tensile Strain at Maximum Load (%)	1438.90	1351.51	1094.95	819.70	542.45
Tensile Extension at Maximum Load (mm)	474.84	446.00	361.33	270.50	179.00
Maximum Stretch	14.77	13.49	10.75	8.34	6.31

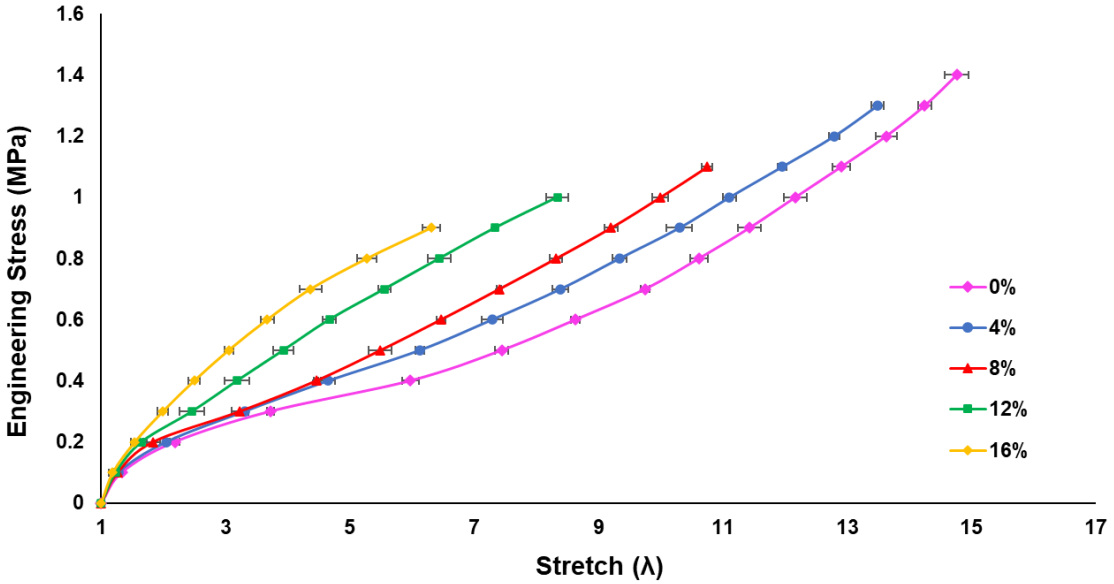

Fig. 2. The engineering stress-stretch curves for the various fiber compositions of *Hevea brasiliensis* - silicone biocomposite

The variance of the stretch values was calculated and found to be between 0% and 4.02%. This shows that the experiment was performed consistently and under control with variance less than 5%. The variances are displayed in Table 3.

Table 3. Standard Deviation and Variance Values

	0%			4%			8%			12%			16%		
	Stretch	Std Dev	Variance	Stretch	Std Dev	Variance	Stretch	Std Dev	Variance	Stretch	Std Dev	Variance	Stretch	Std Dev	Variance
0	1.00	0.000	0.00%	1.00	0.000	0.00%	1.00	0.000	0.00%	1.00	0.000	0.00%	1.00	0.000	0.00%
0.1	1.33	0.023	0.05%	1.28	0.024	0.06%	1.26	0.067	0.45%	1.23	0.018	0.03%	1.19	0.066	0.43%
0.2	2.18	0.079	0.62%	2.05	0.050	0.25%	1.84	0.106	1.12%	1.65	0.027	0.07%	1.54	0.065	0.43%
0.3	3.73	0.058	0.33%	3.31	0.020	0.04%	3.23	0.140	1.96%	2.46	0.197	3.89%	1.99	0.082	0.67%
0.4	5.97	0.136	1.85%	4.65	0.114	1.29%	4.46	0.030	0.09%	3.18	0.193	3.73%	2.50	0.088	0.77%
0.5	7.45	0.107	1.14%	6.13	0.076	0.58%	5.49	0.187	3.50%	3.93	0.160	2.57%	3.05	0.071	0.51%
0.6	8.63	0.068	0.46%	7.29	0.167	2.79%	6.46	0.072	0.52%	4.67	0.107	1.15%	3.67	0.106	1.11%
0.7	9.75	0.074	0.54%	8.39	0.125	1.57%	7.40	0.034	0.12%	5.56	0.097	0.93%	4.37	0.180	3.25%
0.8	10.62	0.147	2.17%	9.34	0.116	1.35%	8.32	0.096	0.93%	6.44	0.190	3.61%	5.27	0.154	2.37%
0.9	11.43	0.186	3.46%	10.30	0.201	4.02%	9.20	0.107	1.13%	7.34	0.026	0.07%	6.31	0.142	2.03%
1	12.17	0.182	3.30%	11.11	0.108	1.17%	9.99	0.126	1.58%	8.34	0.173	2.98%			
1.1	12.91	0.144	2.08%	11.96	0.074	0.54%	10.75	0.082	0.67%						
1.2	13.63	0.167	2.79%	12.80	0.086	0.75%									
1.3	14.25	0.100	1.01%	13.49	0.100	1.01%									
1.4	14.77	0.192	3.69%												

Morphological Characteristics

Fractured surface morphology after tensile testing was analyzed *via* SEM (Fig. 3).

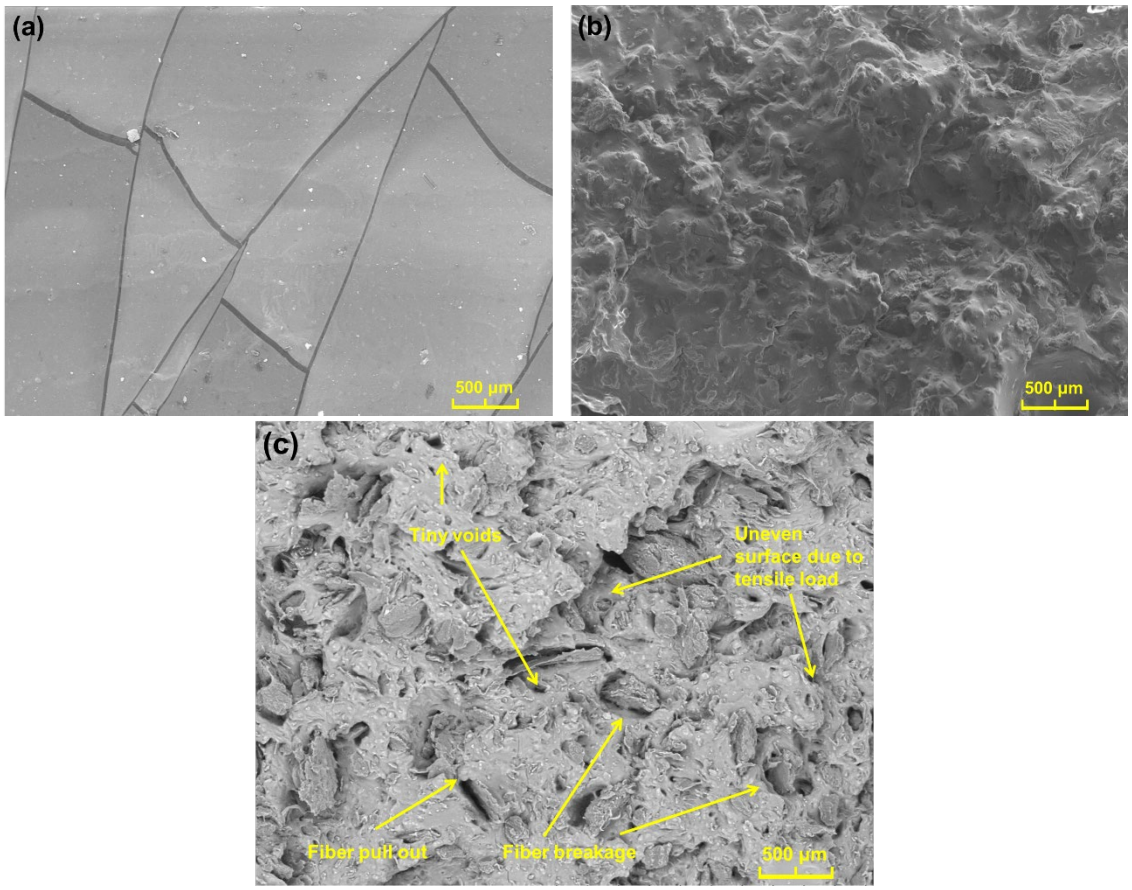

Fig. 3. The SEM micrographs of composite (a) without fibers (b) with a fiber content of 8 wt% (c) with a fiber content of 16 wt%

Specific details, *e.g.*, the dispersion of fibers and failure pattern of the specimens, were visualized. Figure 3a displays a flat, smooth, and clear glass-like surface, while Fig. 3b shows a coarse and rough surface. The surface continued to become rougher as 16 wt% of fiber content was incorporated (Fig. 3c). The smooth and flat surface meant that the pure silicone rubber had low resistance to deformation compared to after the addition of fibers into it. The surface became uneven as the fracture was forced to follow a distorted path due to a barrier induced by the fibers, which resisted breakage. Chen *et al.* (2015) also reported the same when they highlighted the fractured surface morphology of specimens with various volume fractions of phosphor in silicone rubber. It was noticed that the 0 vol. % specimen displayed a smooth, even surface and as the volume fraction of phosphor increased. The surfaces started to become rougher and the distance between the phosphor particles were seen to decrease gradually. The cited authors added that the phenomenon is due to interphase debonding, leading to cracks and voids as the composition of phosphor increases, which indirectly shortens the elongation of composite. A similar phenomenon was highlighted by Shahroze *et al.* (2018), where the composite without nanoclay showed a smoother surface when compared to the composite with nanoclay. As shown in Fig. 3a, there was no void in the pure silicone rubber, which meant that there were no air bubbles trapped inside the specimen. For the specimen with a fiber content of 16 wt%, a few tiny voids were observed. These were either due to air trapped inside the fibers or the fibers being pulled out of the composite.

Hyperelastic Material Constants

Figure 4 highlights the nonlinear elastic behavior of the *Hevea brasiliensis*-silicone biocomposite at different fiber compositions. The best fit curves for the Neo-Hookean, Mooney-Rivlin and Ogden hyperelastic models that mimicked the composite behavior were included.

From Fig. 4, the hyperelastic models used were better at mimicking the curves of composites at higher fiber compositions. At a fiber content of 0 wt%, due to the highly nonlinear elastic behavior of the silicone rubber, the models were unable to accurately mimic the experimental data. A similar result was highlighted by Martins *et al.* (2006), where the Neo-Hookean model that was used poorly mimicked the highly nonlinear pattern. However, as the fiber content increased, the silicone biocomposite behaved in a less nonlinear manner, which allowed the models to better mimic the data.

Between the three models, the Ogden model performed slightly better than the Mooney-Rivlin and Neo-Hookean models. The fitted curves were shown to coincide with the experimental data. This might be due to the limitation of the Neo-Hookean model only having a single material parameter (C_1), while the Mooney-Rivlin and Ogden models have two material parameters, (C_1 and C_2) and (μ and α), respectively.

Coefficient of determination (R^2) values were calculated, where a value of 1 indicates a perfect fit. The closer the value to 1, the higher the degree of accuracy of model in representing the behavior of the curve. The Ogden model showed the highest accuracy with R^2 values ranging from 0.9907 to 0.9991, then followed by Mooney-Rivlin and Neo-Hookean models.

Figure 5 displays the R^2 values for hyperelastic models at different fiber compositions.

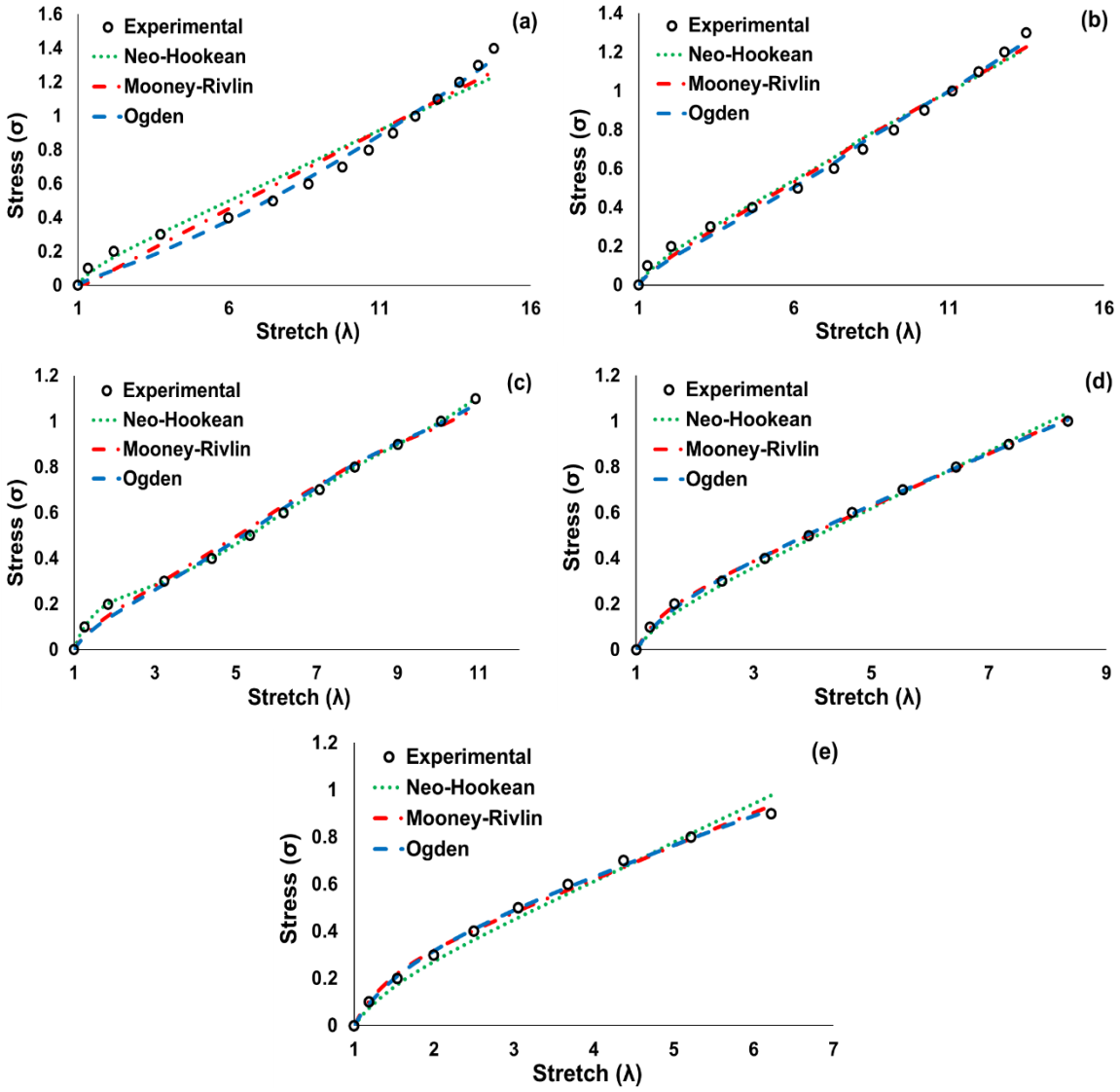

Fig. 4. The stress - stretch curves of the biocomposite at different fiber compositions: (a) 0 wt%, (b) 4 wt%, (c) 8 wt%, (d) 12 wt% and (e) 16 wt%

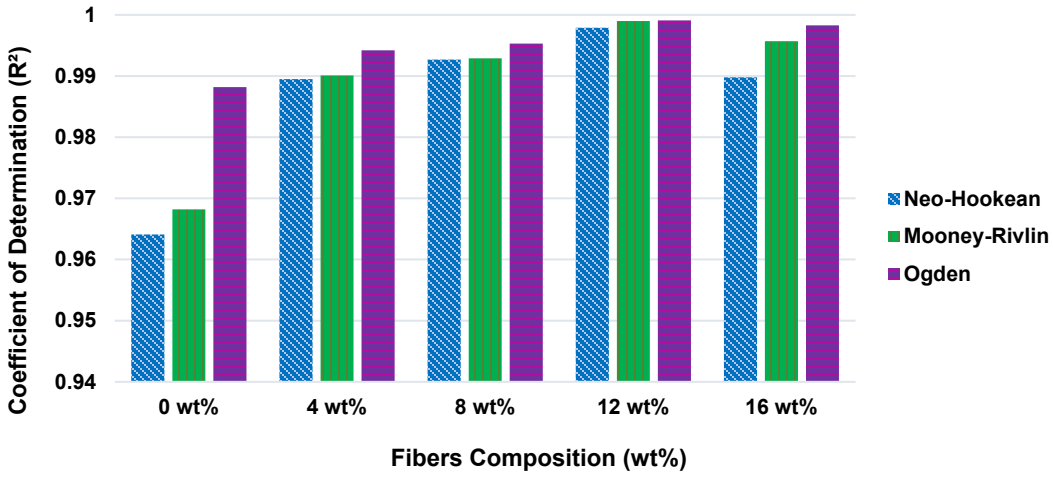

Fig. 5. Coefficient of determination, R² values of each hyperelastic models

A study by Sasso *et al.* (2008) stated that the Mooney-Rivlin and Ogden models accurately demonstrated the rubber-like behavior according to the experimental results. The graphs by Sasso *et al.* (2008) exhibited similar patterns with the current study. (Raheem and Al-Mukhtar 2020) investigated on hyperelastic behavior of hydrogel, where the Ogden, Neo-Hookean, Mooney-Rivlin, and Yeoh models were used to mimic the experimental data. Their findings suggested that the Ogden model was the best choice in representing the nonlinear behavior of the hydrogel due to its stability at small and large strain values. Table 4 shows the material constant values quantified using the three models.

Table 4. Material Constants for *Hevea brasiliensis*-Silicone Biocomposite

Models	Neo-Hookean	Mooney-Rivlin	Ogden
0 wt%	C_1 = 0.04172	C_1 = 0.04619 C_2 = -0.05061	α = 2.3885 μ = 0.03177
4 wt%	C_1 = 0.04518	C_1 = 0.04647 C_2 = -0.01291	α = 2.1231 μ = 0.06756
8 wt%	C_1 = 0.04897	C_1 = 0.04942 C_2 = -0.00350	α = 2.0781 μ = 0.08291
12 wt%	C_1 = 0.06229	C_1 = 0.05734 C_2 = 0.02899	α = 1.8900 μ = 0.15257
16 wt%	C_1 = 0.07781	C_1 = 0.06639 C_2 = 0.04986	α = 1.7808 μ = 0.21942

Table 5. Comparison of Neo-Hookean Material Constant Values of Current Study with Previous Research

C_1	Specimen	Reference
5kPa	Pulmonary Artery Tissue	(Wiltsey *et al.* 2013)
0.8 to 1.7 kPa 2.1 to 3.5 kPa	Human Orbital Fat & Connective Tissue in eye (OFCT)	(Kao *et al.* 2011)
21.7 to 73.9 kPa	Elastomers	(Carpi and Gei 2013)
26.83 to 30.81 kPa	Arenga pinnata/Silicone Biocomposite	(Bahrain *et al.* 2018)
32 to 53 kPa	Kenaf/Silicone Biocomposite	(Noor *et al.* 2015)
41.72 kPa	Silicone Ecoflex 00-30	Current Study
45.18 to 78.41 kPa	Hevea brasiliensis Silicone Biocomposite	Current Study
123.8 to 142.1 kPa	Elastin	(Chen and Weiland 2011)
0.651 MPa to 1 MPa	Thin Polymer Layers	(Chen and Diebels 2012)
2.62 MPa	Polyvinyl Alcohol Sponge	(Karimi *et al.* 2014)
6.81 to 8.51 MPa	Fresh goat skin shaved	(Kim *et al.* 2012)
14.23 to 24.67 MPa	Goat Leather	(Kim *et al.* 2012)
21.88 MPa	Bovine Leather	(Kim *et al.* 2012)

A straightforward pattern could be seen, such that as the fiber content increased, the material constant value increased. The increment of material constant values was in line with the increasing stiffness property of the specimens. For the Ogden model, it could be observed that there was a decrement-increment pattern between the material constants, α and μ values with increasing fiber content. As the fiber content was further increased, the value of α started to decrease gradually while the μ value started to increase gradually. The values of material constants obtained in this study were then compared to other previous

findings. Tables 5 to 7 show the comparison for the Neo - Hookean, Mooney - Rivlin, and Ogden hyperelastic models respectively.

Table 6. Comparison of Mooney-Rivlin Material Constant Values of Current Study with Previous Research

C_1	C_2	Specimen	Reference
-.50 to -2.7 kPa	3.8 to 7.1 kPa	Human Orbital Fat and Connective Tissue in eye (OFCT)	(Kao *et al.* 2011)
17.97 kPa	11.3 kPa	Nylon + Silicone (Ecoflex)	(Guan *et al.* 2004)
20 to 25 kPa	72 to 111 kPa	Kenaf/Silicone Biocomposite	(Noor *et al.* 2015)
31.04 to 39.07 kPa	-123.4 to – 1.71 kPa	Arenga pinnata/Silicone Biocomposite	(Bahrain *et al.* 2018)
46.19 kPa	-50.61 kPa	Silicone Ecoflex 00-30	Current Study
46.47 to 66.39 kPa	-12.91 to 49.86 kPa	Hevea brasiliensis Silicone Biocomposite	Current Study
0.3 MPa	0 MPa	Human Skin	(Polyzois *et al.* 2000)
0.5 MPa	0 MPa	Silicone Rubber (B452)	(Polyzois *et al.* 2000)
1.0 MPa	0.9 MPa	Silicone Rubber (Sil8800)	(Polyzois *et al.* 2000)
8.6240 MPa	2.9634 MPa	Acrylic Elastomer	(Meunier *et al.* 2008)
74.51 to 96.57 Mpa	-88.61 MPa to 109.24 MPa	Fresh goat skin shaved	(Kim *et al.* 2012)
113.28 to 172.44 MPa	-110.55 to 157.78 MPa	Goat Leather	(Kim *et al.* 2012)
164.37 MPa	-157.22 MPa	Bovine Leather	(Kim *et al.* 2012)

Table 7. Comparison of Ogden Material Constant Values of Current Study with Previous Research

Shear Modulus, μ	Strain hardening component, α	Specimen	Reference
10 Pa	110	Human Skin (Ventral Forearm)	(Mahmud *et al.* 2012)
31.77 kPa	2.389	Silicone Ecoflex 00-30	Current Study
67.56 to 219.42 kPa	1.781 to 2.123	Hevea brasiliensis Silicone Biocomposite	Current Study
0.11 MPa	9	Human Skin	(Polyzois *et al.* 2000)
0.152 to 0.277 MPa	16.16 to 17.31	Fresh goat skin shaved	(Kim *et al.* 2012)
1.827 MPa	15.89	Goat Leather	(Kim *et al.* 2012)
3.50 MPa	14.82	Bovine Leather	(Kim *et al.* 2012)

The increasing material constants indicate a stiffer and harder to break material. (Bahrain *et al.* 2018) incorporated 12 wt% of *Arenga pinnata* fiber into silicone rubber to study its tensile behavior. The data were used to determine the material constant values by employing two hyperelastic models which were Neo-Hookean and Mooney-Rivlin models. The material constant values obtained were $C1$ = 0.03081 (Neo-Hookean) and C_1 = 0.03104, C_2 = -0.00171 for the Mooney-Rivlin model. By referring to Table 5, it can be

seen that the material constant values generated for 12 wt% of *Hevea brasiliensis*-silicone biocomposite were higher for both of the models. This indicated that the 12 wt% of *Hevea brasiliensis*-silicone biocomposite was stiffer than the 12 wt% of *Arenga pinna*/silicone composite.

(Noor *et al.* 2015) in their study incorporated kenaf fiber into silicone rubber of up to 25 phr (part per hundred part of silicone rubber), which was equivalent to 25 wt% fiber in this study. Neo-Hookean and Mooney-Rivlin hyperelastic models were also employed to investigate its tensile properties. At 25 phr of kenaf fiber amount, the material constant values were $C_1 = 0.053$ (Neo-Hookean), and $C_1 = 0.025$, $C_2 = 0.111$ for the Mooney-Rivlin model. Even at 25 phr, the material constant values generated for the kenaf/silicone composite were less than the material constant values generated for 16 wt% of *Hevea brasiliensis*-silicone biocomposite. Hence, it can be said that the *Hevea brasiliensis* fiber used in this study is far stronger and more resilient than the kenaf and *Arenga pinnata* fibers. However, both studies do not include the values of coefficient of determination. Therefore, the accuracy of the curve fitting cannot be known.

CONCLUSIONS

1. Modulus of material increased as the silicone rubber was reinforced by an increasing fiber content. This is supported by the increasing material constant values. However, the elasticity and flexibility decreased as shown by the decreasing maximum elongation and stretch values.
2. The scanning electron micrographs (SEM) highlighted the change in morphology of the fractured surfaces of the specimens. It was shown that pure silicone possessed a smooth surface and as the fiber content increased, the fractured surfaces of the specimens became rough. This supported the increasing modulus value of the silicone biocomposites.
3. From the numerical analyses, the Ogden model better represented the deformation behavior of biocomposites over Mooney-Rivlin and Neo-Hookean models.

ACKNOWLEDGMENTS

This work was funded by the Ministry of Education, Malaysia and the Universiti Teknologi MARA. (Fundamental Research Grant Scheme, Grant No. 600–IRMI/FRGS 5/3 (102/2017). Hevea brasiliensis – silicone biocomposite has been copyrighted as HeBraC; IP no. CRLY00026192 with the Intellectual Property Corporation of Malaysia (MyIPO).

REFERENCES CITED

ASTM D412 (2008). "Standard test methods for vulcanized rubber and thermoplastic elastomers - Tension," ASTM International, West Conshohocken, PA.

Ali, A., Sahari, B. B., and Hosseini, M. (2010). "A review of constitutive models for rubber-like materials," *American Journal of Engineering and Applied Sciences* 3(1), 232-239. DOI:10.3844/ajeassp.2010.232.239

Bahrain, S. H. K., Mahmud, J., and Ismail, M. H. (2018). "*Arenga pinnata*–Silicone biocomposite properties via experimental and numerical analysis," *Materials Science* 24(3), 277-282. DOI: 10.5755/j01.ms.24.3.18296

Benevides, R. O., and Nunes, L. C. S. (2015). "Mechanical behavior of the alumina-filled silicone rubber under pure shear at finite strain," *Mechanics of Materials: An International Journal* 85, 57-65. DOI: 10.1016/j.mechmat.2015.02.011

Carpi, F., and Gei, M. (2013). "Predictive stress–stretch models of elastomers up to the characteristic flex," *Smart Materials and Structures* 22(10), article no. 104011. DOI:10.1088/0964-1726/22/10/104011

Chen, K., and Weiland, J. D. (2011). "Mechanical properties of orbital fat and its encapsulating connective tissue," *Journal of Biomechanical Engineering* 133(6). DOI:10.1115/1.4004289

Chen, X., Wang, S., Cao, C., and Liu, S. (2015). "Influence of phosphor amount on microstructure and damage evolution of silicone/phosphor composite in light-emitting diodes packaging," *Composites Science and Technology* 107, 98-106. DOI: 10.1016/j.compscitech.2014.12.004

Chen, Z., and Diebels, S. (2012). "Nanoindentation of hyperelastic polymer layers at finite deformation and parameter re-identification," *Archive of Applied Mechanics* 82(8), 1041-1056. DOI: 10.1007/s00419-012-0613-9

Feng, L., Li, S. and Feng, S. (2017). "Preparation and characterization of silicone rubber," *RSC Adv. Royal Society of Chemistry* (22), 13130-13137. DOI: 10.1039/c7ra00293a

Guan, E., Smilow, S., Rafailovich, M., and Sokolov, J. (2004). "Determining the mechanical properties of rat skin with digital image speckle correlation," *Dermatology* 208(2), 112-119. DOI: 10.1159/000076483

Hanipah, S. H., Omar, F. N., Talib, A. T., Mohammed, M. A. P., Baharuddin, A. S., and Wakisaki, M. (2020). "Effect of silica bodies on oil palm fiber-polyethylene composites," *BioResources* 15(1), 360-367. DOI: 10.15376/biores.15.1.360-367

Haque, A., Mondal, D., Khan, I., Usmani, A.M., Bhat, A. H., and Gazal, U. (2017). "Fabrication of composites reinforced with lignocellulosic materials from agricultural biomass," in *Lignocellulosic Fibre and Biomass-Based Composite Materials*, pp. 179-191. DOI: 10.1016/B978-0-08-100959-8.00010-X

Haris, N. F. N., Mahmud, J., and Yahaya, M. A. (2019). "Quantifying the tensile properties of *Hevea brasiliensis* – Silicone biocomposite using Neo – Hookean model," *International Journal of Recent Technology and Engineering* 8(4), 6939-6943. DOI: 10.35940/ijrte.d5181.118419

Haris, N. I. N., Hassan, M. Z., Ilyas, R. A., Suhot, M. A., Sapuan, S. M., Dolah, R., Mohammad, R., and Asyraf, M. R. M. (2022). "Dynamic mechanical properties of natural fiber reinforced hybrid polymer composites: A review," *Journal of Materials Research and Technology* 19, 167-182. DOI: 10.1016/j.jmrt.2022.04.155

Helaili, S., Chafra, M., and Chevalier, Y. (2021). "Natural fiber alfa/epoxy randomly reinforced composite mechanical properties identification," *Structures* 34, 542-549. DOI: 10.1016/j.istruc.2021.07.095

Ismail, A. M., Mahmoud, K. R. and Salam, M. H. A. (2015). "Electrical conductivity and positron annihilation characteristics of ternary silicone rubber/carbon black/TiB2 nanocomposites," *Polymer Testing* 48, 37-43. DOI: 10.1016/j.polymertesting.2015.09.006

Kao, P. H., Lammers, S. R., Tian, L., Hunter, K., Stenmark, K. R., Shandas, R., and Qi, H. J. (2011). "A microstructurally driven model for pulmonary artery tissue," *Journal of Biomechanical Engineering* 133(5), article no. 051002. DOI:10.1115/1.4002698

Karimi, A., Navidbakhsh, M., and Beigzadeh, B. (2014). "A visco-hyperelastic constitutive approach for modeling polyvinyl alcohol sponge," *Tissue and Cell* 46(1), 97-102. DOI: 10.1016/j.tice.2013.12.004

Khan, A. S., Man, Z., Bustam, M. A., Kait, C. F., Ullah, Z., Nasrullah, A., Khan, M. I., Gonfa, G., Ahmad, P., and Muhammad, N. (2016). "Kinetics and thermodynamic parameters of ionic liquid pretreated rubber wood biomass," *Journal of Molecular Liquids* 223, 754-762. DOI: 10.1016/j.molliq.2016.09.012

Kim, B., Lee, S. B., Lee, J., Cho, S., Park, H., Yeom, S., and Park, S. H. (2012). "A comparison among Neo-Hookean model, Mooney-Rivlin model, and Ogden model for chloroprene rubber," *International Journal of Precision Engineering and Manufacturing* 13(5), 759-764. DOI:10.1007/s12541-012-0099-y

Lima, M. M. D. S., and Borsali, R. (2004). "Rodlike cellulose microcrystals: Structure, properties, and applications," *Macromolecular Rapid Communications* 25(7), 771-787. DOI: 10.1002/marc.200300268

Mahmud, J., Evans, S. L., and Holt, C. A. (2012). "An innovative tool to measure human skin strain distribution in vivo using motion capture and delaunay mesh," *Journal of Mechanics* 28(2), 309-317. DOI:10.1017/jmech.2012.34

Martins, P. A. L. S., Jorge, R. M. N., and Ferreira, A. J. M. (2006). "A comparative study of several material models for prediction of hyperelastic properties: Application to silicone-rubber and soft tissues," *Strain* 42(3), 135-147. DOI: 10.1111/j.1475-1305.2006.00257.x

Meunier, L., Chagnon, G., Favier, D., Orgéas, L., and Vacher, P. (2008). "Mechanical experimental characterisation and numerical modelling of an unfilled silicone rubber," *Polymer Testing* 27(6), 765-777. DOI: 10.1016/j.polymertesting.2008.05.011

Moon, R. J., Martini, A., Nairn, J., Simonsen, J., and Youngblood, J. (2011). "Cellulose nanomaterials review: Structure, properties and nanocomposites," *Chemical Society reviews* 40(7), 3941-3994. DOI: 10.1039/c0cs00108b

Noor, S. N. A. M., Khairuddin, M. A. F., and Mahmud, J. (2015). "Biocomposite silicone: Synthesis, mechanical testing and analysis," *New Developments in Mechanics and Mechanical Engineering* 1(1), 113-117.

Petchpradab, P., Yoshida, T., Charinpanitkul, T., and Matsumura, Y. (2009). "Hydrothermal pretreatment of rubber wood for the saccharification process," *Industrial & Engineering Chemistry Research* 48(9), 4587-4591. DOI: 10.1021/ie801314h

Polyzois, G. L., Tarantili, P. A., Frangou, M. J., and Andreopoulos, A. G. (2000). "Physical properties of a silicone prosthetic elastomer stored in simulated skin secretions," *The Journal of Prosthetic Dentistry* 83(5), 572-577. DOI: 10.1016/s0022-3913(00)70017-5

Radzi, N. S. M. and Mahmud, J. (2017). "Sealing capability and hyperelastic behaviour of silicone biocomposites via compression test," *Materialwissenschaft und Werkstofftechnik* 48(3–4), 311–317. DOI: 10.1002/mawe.201700008

Raheem, H. M., and Al-Mukhtar, A. M. (2020). "Experimental and analytical study of the hyperelastic behavior of the hydrogel under unconfined compression," *Procedia Structural Integrity* 25, 3-7. DOI: 10.1016/j.prostr.2020.04.002

Ratnasingam, J., Ramasamy, G., Wai, L. T., Senin, A. L., and Muttiah, N. (2015). "The prospects of rubberwood biomass energy production in Malaysia," *BioResources* 10(2), 2526-2548. DOI: 10.15376/biores.10.2.2526-2548

Raza, M. A., Westwood, A., Brown, A., Hondow, N., and Stirling, C. (2011). "Characterisation of graphite nanoplatelets and the physical properties of graphite nanoplatelet/silicone composites for thermal interface applications," *Carbon* 49(13), 4269-4279. DOI: 10.1016/j.carbon.2011.06.002

Sasso, M., Palmieri, G., Chiappini, G., and Amodio, D. (2008). "Characterization of hyperelastic rubber-like materials by biaxial and uniaxial stretching tests based on optical methods," *Polymer Testing* 27(8), 995-1004. DOI: 10.1016/j.polymertesting.2008.09.001

Shaaban, A., Se, S.-M., Mitan, N. M. M., and Dimin, M. F. (2013). "Characterization of biochar derived from rubber wood sawdust through slow pyrolysis on surface porosities and functional groups," *Procedia Engineering* 68, 365-371. DOI: 10.1016/j.proeng.2013.12.193

Shaaban, A., Se, S.-M., and Ahsan, Q. (2015). "Preparation of rubber wood sawdust-based activated carbon and its use as a filler of polyurethane matrix composites for microwave absorption," *New Carbon Materials. Institute of Coal Chemistry, Chinese Academy of Sciences* 30(2), 167-175. DOI: 10.1016/S1872-5805(15)60182-2

Shahroze, R. M., Ishak, M. R., Salit, M. S., Leman, Z., Asim, M., and Chandrasekar, M. (2018). "Effect of organo-modified nanoclay on the mechanical properties of sugar palm fiber-reinforced polyester composites," *BioResources* 13(4), 7430-7444. DOI: 10.15376/biores.13.4.7430-7444

Sulaiman, O., Nasir, M., Hashim, R., Nordin, M. A., and Asim, M. (2015). "Improved physical and chemical properties of rubber wood (*Hevea brasiliensis*) fiber by laccase," *Asian Journal of Agricultural Research. Science Alert* 9(4), 166-172. DOI: 10.3923/ajar.2015.166.172

Wang, L., and Cheng, L. (2014). "Piezoresistive effect of a carbon nanotube silicone-matrix composite," *Carbon* 71, 319-331. DOI: 10.1016/j.carbon.2014.01.058

Wiltsey, C., Kubinski, P., Christiani, T., Toomer, K., Sheehan, J., Branda, A., and Vernengo, J. (2013). "Characterization of injectable hydrogels based on poly(N-isopropylacrylamide)-g-chondroitin sulfate with adhesive properties for nucleus pulposus tissue engineering," *Journal of Materials Science: Materials in Medicine* 24, 837-847. DOI 10.1007/s10856-013-4857-x

Wu, Y. and Yu, Z. (2015). "Thermal conductivity of in situ epoxy composites filled with ZrB2 particles," *Composites Science and Technology* 107, 61-66. DOI: 10.1016/j.compscitech.2014.12.007

Xu, Q., Pang, M., Zhu, L., Zhang, Y., and Feng, S. (2010). "Mechanical properties of silicone rubber composed of diverse vinyl content silicone gums blending," *Materials in Engineering* 31(9), 4083-4087. DOI: 10.1016/j.matdes.2010.04.052

Xu, Y., Gao, Q., Liang, H., and Zheng, K. (2016). "Effects of functional graphene oxide on the properties of phenyl silicone rubber composites," *Polymer Testing* 54, 168-175. DOI: 10.1016/j.polymertesting.2016.07.013

Article submitted: March 19, 2020; Peer review completed: April 2, 2020; Revised version received and accepted: May 30, 2022; Published: June 14, 2022.
DOI: 10.15376/biores.17.3.4623-4637